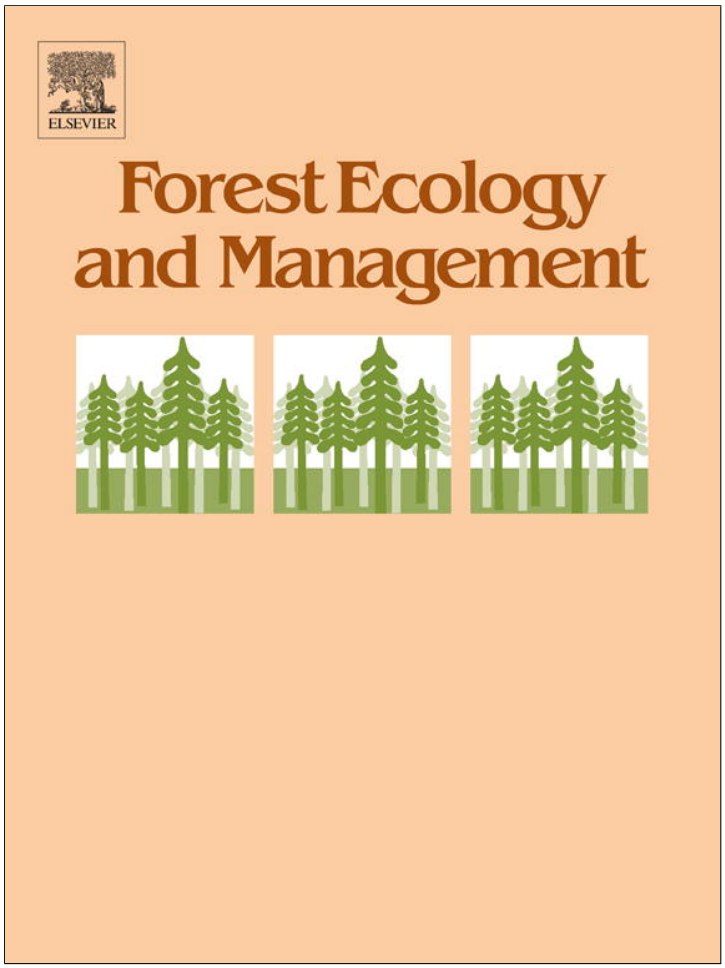

(This is a sample cover image for this issue. The actual cover is not yet available at this time.)

Forest Ecology and Management 279 (2012) 97–111

Contents lists available at SciVerse ScienceDirect

Forest Ecology and Management

journal homepage: www.elsevier.com/locate/foreco

Spatio-temporal prediction of site index based on forest inventories and climate change scenarios

Arne Nothdurft [a,*], Thilo Wolf [a], Andre Ringeler [b], Jürgen Böhner [b], Joachim Saborowski [c]

[a] Forest Research Institute Baden-Württemberg, Department of Biometrics and Informatics, Germany
[b] University of Hamburg, Institute of Geography, Germany
[c] University of Göttingen, Department of Ecoinformatics, Biometrics and Forest Growth and Department of Ecosystem Modelling, Germany

ARTICLE INFO

Article history:
Received 22 February 2012
Received in revised form 10 May 2012
Accepted 11 May 2012

Keywords:
Site-index prediction
Climate change
Forest inventory

ABSTRACT

A methodological framework is provided for the quantification of climate change effects on site index. Spatio-temporal predictions of site index are derived for six major tree species in the German state of Baden-Württemberg using simplified universal kriging (UK) based on large data sets from forest inventories and a climate sensitive site-index model. It is shown by a simulation study that, with the underlying large sample size, residual kriging using ordinary least squares (OLS) estimates of the mean function leads to an approximately unbiased spatial predictor. Moreover, the simulated coverage probabilities of resulting prediction intervals are quite close to the required level. B-spline regression techniques are applied to model nonlinear cause-and-effect curves for estimating site indexes at existing inventory plots dependent on retrospective climate covariates. The spatially structured error is modeled by exponential covariance functions. The mean model is then applied to downscaled climate projection data to spatially predict the relative changes of site index under perturbed climate conditions.

Applying climate projections of an existing regional climate model based on IPCC emission scenarios A1B and A2, it is found that site index of all tree species would be decreased in lowland areas, and may increase in mountainous regions. Silver fir and common oak stands would also show increased site indexes in mountainous regions, but further extended to lower elevation levels. Site conditions in the Alpine foothills may remain highly productive for growth of Norway spruce, Baden-Württemberg's most dominant tree species. Whereas site index of common beech and Douglas-fir may decrease to almost the same relative amount and on nearly the same sites as Norway spruce, site index of Scots pine may be less affected by future climate change.

1. Introduction

The effects of climate change caused by atmospheric emissions of greenhouse gases are assumed to increase more rapidly than forests might react on the strength of their natural adaption potential in terms of phenotypic plasticity, evolution or migration (Iverson and Prasad, 1998, 2000). Therefore, human intervention is necessary to improve adaptiveness and to assure future productivity of managed forests. It was found that global warming has already led to extended growing seasons in the recent past (Menzel and Fabian, 1999; Chmielewski and Rötzer, 2001), but may also cause growth depression due to droughts, especially in conjunction with shifting precipitation sums from summer to winter months. That means, for regions with heterogeneous topography such as Baden-Württemberg (Fig. 1) the effects of climate change may result in both, reduced and increased productivity depending on sites; see the findings in Latta et al. (2010) for United States Pacific Northwest. Concluding from existing knowledge about vegetation ecology (Ellenberg, 2009) climate change will have unequal effects on the different tree species. Because of long rotation periods usually applied in sustainable forest management, long-term prognoses such as shown in Lindner et al. (2000) and in Köhl et al. (2010) are now required to support practitioner's decisions on the optimal choice of certain tree species compositions for replantings.

Our study provides prognoses showing where and to which amount and direction site index of certain tree species could change as a response to future climate trends in the German state of Baden-Württemberg. Like in the paper by Albert and Schmidt (2010), site index, which is the dominant height at certain reference age, is applied here as an indicator for site productivity. According to the traditional site-index concept two models are built, an age dependent dominant height growth model and another regression model for site index dependent on climate and topographic variables. The dominant height growth model is fitted to repeated measurements from regional forest inventories

* Corresponding author.
E-mail addresses: arne.nothdurft@forst.bwl.de (A. Nothdurft), thilo.wolf@forst.bwl.de (T. Wolf), aringel@saga-gis.org (A. Ringeler), boehner@geowiss.uni-hamburg.de (J. Böhner), jsaboro@gwdg.de (J. Saborowski).

0378-1127/$ - see front matter © 2012 Elsevier B.V. All rights reserved.
http://dx.doi.org/10.1016/j.foreco.2012.05.018

Fig. 1. Geographical regions of Baden-Württemberg located in Southwest Germany.

and used to estimate current site index of inventory plots by height growth projections. The site-index model is fitted to these growth projections on all sample plot locations of regional inventories as well as of the German national forest inventory in Baden-Württemberg.

The site-index model is based on nonparametric B-spline regression producing biologically plausible cause-and-effect curves of parabolic shape (Kahn, 1995). Our approach to spatial prediction of site index was inspired by Mandallaz (1993) who adopted geostatistical methods to forest inventory. It is based on a simplified universal kriging (UK) with the site-index model used as the mean function and an exponential autocorrelation function for the random spatial variation component. The huge amount of observations from forest inventories inhibits the application of iteratively re-weighted generalized least squares (IRWGLS), which is often applied to account for spatial correlation. However, we hypothesized for this study that OLS-residuals (first step of IRWGLS) are sufficient for reliable estimation of spatial process parameters and also for spatial predictions based on residual kriging if large data sets from forest inventories are available. Using exhaustive simulations of Gaussian random fields it is examined, whether OLS in conjunction with residual kriging yields approximately unbiased parameter estimates of the semi-variogram function, approximately unbiased spatial predictions, and, finally, predefined coverage rates of estimated prediction intervals.

The major two aims of this study are (i) to provide spatio-temporal predictions of site index for different climate scenarios in Baden-Württemberg, and (ii) to provide a statistically sound and easy to implement approach to model the effects of climate change on site index using large data sets from forest inventories and climate projections.

2. Material

2.1. Climate data

2.1.1. Retrospective climate data

Regression modeling of site index is based on retrospective climate data for the period between 1971 and 2007. Daily resolution values of climatic variables on a 50 m × 50 m grid were derived by a hierarchical model chain, which merges statistical and dynamical downscaling steps. Large-scale atmospheric processes of the recent climate system were represented by NCAR/NCEP reanalysis series (Kalnay et al., 1996), defining lateral boundary conditions at the top of the model chain in a coarse grid resolution of 2.5° × 2.5° (latitude/longitude). To take into account mesoscale atmospheric processes, dynamical downscaling was performed in two consecutive downscaling steps using the nonhydrostatic regional climate model Weather Research and Forecasting (WRF) (Skamarock et al., 2005; Langkamp and Böhner, 2011). In the first downscaling step results were produced in a 30 km × 30 km grid resolution for an extended area, broader than Baden-Württemberg's territory, to sufficiently depict synoptic scale processes (e.g. fronts and disturbances). The second step was restricted to the actual Baden-Württemberg region and yielded gridded data of 5 km × 5 km resolution, in which most of the regional-scale features of the boundary layer were sufficiently considered.

To bridge the spatial scale gap between the coarse grid-point representation of the WRF and the needs for local scale climate information for regression modeling of site index, a further statistical downscaling scheme was implemented. Meteorological observations from the met-station network of the German National Meteorological Service (Deutscher Wetterdienst, DWD) were linked to WRF circulation variables using multivariate statistical analysis to define robust transfer functions. Assuming that spatial and temporal variability of climatic variables is predominantly controlled by both, mesoscale synoptic modes and surface-forced sub-synoptic processes, the applied approach directly integrates local and complex surface parameters in the exploitation of transfer functions (cf. Böhner and Antonić, 2008) and thus enabled a final downscaling to produce climate layers with high resolution of 50 m × 50 m grid width, sufficiently accounting for local topographic settings and the specific surface heterogeneity in Baden-Württemberg.

However, to guarantee that the downscaling results were consistent with actual local weather recordings, a final bias correction was applied using a kernel smoother and the local residuals obtained from the deviation between the downscaled climate layers and long-term daily met-station observations. For a more detailed description of the statistical downscaling approach the reader is referred to Böhner (2006) and Böhner and Antonić (2008).

The downscaling approach described above was applied to the daily total precipitation, and the average, the maximum and the minimum daily temperature. This led to a total of 13,514 grid data files for each of the four variables representing daily values in 50 m × 50 m spatial resolution and covering the period from 1971 to 2007. However, only the variables daily precipitation and average daily temperature were later used for defining appropriate covariates for regression modeling. Due to strong correlations among the temperature variables, no relevant extra information was provided by the minimum and the maximum temperature.

In the regression models predicting the spatial trend of site index we considered 30-year long-term means, for the period between 1978 and 2007, of total precipitation during the growing season (precipitation or PGS) and the total of average daily temperatures during the growing season (temperature or TGS) as explaining variables. For the definition of the growing season, we followed v.Wilpert's (1990) criteria for the determination of its beginning and duration. He states that the growing season starts if the seven-day moving average daily temperature is greater than or equal to ten degrees centigrade; and growing season stops if either the seven-day moving average daily temperature is less than ten degrees centigrade on five consecutive days or if the limiting-daylight criterion is met, which is set at 6th of October. Once growing season has stopped it may continue again if the seven-day moving

average daily temperature rises above ten degrees centigrade on five consecutive days and as long as the limiting-daylight criterion is not met. In addition to the temperature and the limiting-daylight criteria a third criterion was originally formulated in v.Wilpert (1990) taking into account that tree growth is interrupted by drought if soil moisture tension falls below −1100 hectopascal on five consecutive days. Because so far no information for soil conditions in Baden-Württemberg were available to derive predictions from a water balance model, the drought criterion was omitted for the present study.

For each 50 m × 50 m pixel and each day it was checked whether the criteria were met yielding binary 0/1-grids of the entire region for each day; 1 indicates that tree growth is assumed to occur. Each of the binary grid data files is then multiplied with the corresponding grid containing the downscaled results for the daily precipitation, and the average daily temperature respectively, and from those products cumulative sums were calculated over each calendar year. This procedure resulted in one grid data file per calendar year, wherein each pixel contains the TGS and the PGS. Finally, retrospective 30-year averages for the period between 1978 and 2007 of both climate variables were calculated.

The application of totals during the growing season has the pleasant side effect that correlations among the climate variables are reduced. Whereas correlation between the 30-year long-term average of the total annual precipitation and the 30-year average daily temperature is -47%, correlation is reduced to only -19% when using TGS and PGS as totals during the growing season. The same effect happens to the correlation between the long-term averages of precipitation and elevation above sea level; correlation between elevation and the total annual precipitation is 55% and is reduced to only 32%, when using PGS.

2.1.2. Climate projection data

The climate projection data stem from existing climate simulations performed by the hydrostatic Regional Climate Model (RCM) REMO (Majewski, 1991; Roeckner et al., 1996; Jacob, 2001; Jacob et al., 2001) on initiative of the German Federal Environment Agency (Umweltbundesamt). REMO was forced by lateral boundary conditions of the general circulation model (GCM) ECHAM5-MPIOM (Roeckner et al., 2003) to produce daily climate values in 10 km × 10 km horizontal grid resolution for the scenarios A1B, A2 and B1 from the Special Report on Emissions Scenarios (SRES) (Nakicenovic et al., 2000) of the Intergovernmental Panel on Climate Change (IPCC). REMO projections were spatially refined to grid data files with higher grid resolution of 1 km × 1 km using the same downscaling approach as applied to the retrospective climate data described above.

Due to the coarse resolution of the RCM output and the relatively fine resolution required in our study, it happens that the downscaled grid data files of climate projections show implausible spatial patterns, especially with respect to precipitation, which can be higher than expected in low lands on the windward side of mountains and lower than expected in mountainous terrain. For solution, the easy to apply so-called anomaly approach was used, which means that the climate model's predicted future change in relation to a predefined reference period is added to observed climate time series in the past to yield future climate projections. As the available REMO projection data started in 2001 and retrospective data ended in 2007, the reference period was set to the range from the beginning of 2001 until the end of 2007. Grid data files of seven-year averages of the TGS and of the PGS are therefore calculated with respect to the reference period from 2001 to 2007 for both data sets, the projections and the retrospective data. The difference between both data sets, which can be termed as climate model bias, is finally subtracted from the future projection grid data. The site-index model, developed by the nonparametric regression fit to the retrospective data, is used to estimate site index of inventory plots based on the 30-year averages of PGS and TGS for the two periods [2011,...,2040] and [2041,...,2070].

Table 1
Number of sample plots and trees from the forest inventory data used for fitting the growth model and the site-index model.

Species	Growth model		Site-index model
	Sample plots	Trees	Sample plots
Norway spruce	34,621	57,472	91,642
Silver fir	12,816	19,374	33,987
Douglas-fir	3989	4922	9356
Scots pine	10,376	14,892	31,559
Common/Sessile oak	9690	13,010	28,230
Common beech	28,296	43,410	81,241

2.2. Forest inventory data

The forest inventory data used in this study comprise the sample plot data from Baden-Württemberg regional inventories (BI), and from the German national forest inventories (BWI). In the BI sample plots have been arranged in regular grids of 100 m × 200 m mesh width in the past and of 200 m × 200 m today. The interval between two consecutive measurements in the BI is usually ten years. The sample plots of the BWI were selected using a 2 km × 2 km grid. Different from the wide-meshed BWI plots, which are established in forests of all types of ownership, the BI plots are only established in state forest districts and municipal forests.

The crucial variable for site-index modeling, repeatedly measured on all inventory plots, is dominant height, here of the six major tree species occurring in Baden-Württemberg. These are Norway spruce (*Picea* abies (L.) H.Karst.), silver fir (*Abies* alba Mill.), Douglas-fir (*Pseudotsuga* menziesii Carrière), Scots pine (*Pinus* sylvestris L.), common/sessile oak (*Quercus* robur L./*Quercus petraea* (Mattuschka) Liebl.) and common beech (*Fagus* sylvatica L.). Tree height measurements of the BI are available from 1996 to 2009 (for common/sessile oak from 1994), of the BWI from 1986 or 1987 to 2009 or 2010, depending on the tree species. More recent inventory data were not available for this study, because regional forest inventory is usually performed one year before forest management planning is started, and inventory data files are transfered to the central database not until forest management planning is completed. See Table 1 for the numbers of sample plots and trees with repeated height measurements in the BI. Even for the rarest species, Douglas-fir, there are 4,922 dominant trees with repeated height measurements on 3,989 sample plots. Since site-index projection becomes more uncertain the more stand age differs from the reference age, only sample plots were considered here, on which dominant height tree age is between 40 and 200 years.

The data from both inventory systems were finally pooled and provided with site-index predictions for the interesting future periods covering the entire forest area of Baden-Württemberg. Such predictions are available for Norway spruce at 91,642 forest inventory sample plot locations and at 9,356 sample plot locations for Douglas-fir (Table 1). That pooled data set was then used for spatial predictions of site index by simplified UK.

3. Methods

3.1. Dominant height growth

Earlier work showed that Sloboda's (1971) height growth function

Table 2
Parameter estimates and R^2 (calculated as one minus residual sum of squares divided by total sum of squares) for the dominant height growth model.

Species	ψ_1	ψ_2	ψ_3	R^2
Norway spruce	59.794	0.100	0.465	0.32
Silver fir	61.297	0.400	0.798	0.41
Douglas-fir	75.711	0.249	0.666	0.37
Scots pine	111.175	0.570	1.077	0.22
Common/Sessile oak	82.043	0.167	0.694	0.14
Common beech	68.710	0.072	0.441	0.19

$$h(t) = \psi_1 [h(t_0)/\psi_1]^{\exp\left[\frac{\psi_2}{(\psi_3-1)t^{(\psi_3-1)}} - \frac{\psi_2}{(\psi_3-1)t_0^{(\psi_3-1)}}\right]}, \quad (1)$$

is a good choice for height growth modeling of Norway spruce in Baden-Württemberg (Nothdurft et al., 2006). Here, we obtained the estimates of the ψ-parameters (see Table 2) using nonlinear least squares to fit the first-order derivative form

$$\frac{\partial h(t)}{\partial t} = \psi_2 \frac{h(t)}{t^{\psi_3}} \ln\left(\frac{\psi_1}{h(t)}\right) \quad (2)$$

to the observed dominant height growth increments of the BI, which simply result from the differences between consecutive dominant height measurements of the trees. $h(t)$ was set to the average height and t the average age of the two consecutive measurements.

Site index is now defined as the dominant tree height at reference age t_o = 100 years. For a given observation of dominant height $h(t)$ at age t on an arbitrary sample plot a projection of site index can consequently be achieved by

$$h(t_o|h(t),t) = \psi_1 [h(t)/\psi_1]^{\exp\left[\frac{\psi_2}{(\psi_3-1)t_o^{(\psi_3-1)}} - \frac{\psi_2}{(\psi_3-1)t^{(\psi_3-1)}}\right]}, \quad (3)$$

which describes a set of curves over positive ages t_o. With t given, the two curves for any pair of positive $h(t)$ do not intersect.

3.2. Spatial modeling

The spatial process of site index is here defined for any arbitrary location s in the Baden-Württemberg region W as

$$y(s) = x(s)'\beta + b(s) + \epsilon(s), \quad (4)$$

and is composed of

(i) a fixed linear trend dependent on site and climate variables in $x(s)$,
(ii) a spatially correlated error in terms of a Gaussian process $b(s)$, with 0 mean, variance θ^2, and spatial autocovariance function $c(h)$, h being the distance between two locations s_i and s_j,
(iii) and an unstructured error $\epsilon(s) \sim N(0,\sigma^2)$.

In its vector form

$$y = X\beta + Ub + \epsilon \quad (5)$$

one recognizes the mixed-model formulation of the geostatistical UK model with covariance matrix

$$\mathbb{C}\mathrm{ov}(y) = \Sigma = \theta^2 URU' + \sigma^2 I_n \quad (6)$$

and correlation matrix

$$R = \mathbb{C}\mathrm{orr}[b(s_i), b(s_j)] = \rho(s_i - s_j). \quad (7)$$

After some trials an exponential correlation function $\rho(h) = \exp(-h/\alpha)$ was chosen, leading to the covariance function

$$c(h) = \begin{cases} \theta^2 \exp\left(-\frac{h}{\alpha}\right), & \text{for } h > 0 \\ \sigma^2 + \theta^2, & \text{for } h = 0 \end{cases} \quad (8)$$

and to the parametric semi-variogram model

$$\gamma(h) = \begin{cases} \sigma^2 + \theta^2\left[1 - \exp\left(-\frac{h}{\alpha}\right)\right], & \text{for } h > 0 \\ 0, & \text{for } h = 0. \end{cases} \quad (9)$$

The unstructured error ϵ, which is represented by σ, is termed the nugget effect and mathematically quantifies measurement error.

Universal kriging is often performed as kriging of the residuals $y - X\beta$. However, this causes the well-known circular problem. The estimation of β via GLS requires the autocovariance matrix (Eq. (6)), while an estimate of β is needed to calculate the empirical residuals, which are necessary to estimate the autocovariance matrix. As described in Cressie (1991) and Schabenberger and Gotway (2005) a usual approach to handle the "cat and mouse game of universal kriging" is to apply Neuman and Jacobson's (1984) approach of *iteratively re-weighted generalized least squares* (IRWGLS).

In IRWGLS a prior OLS estimate

$$\hat{\beta}_{OLS} = (X'X)^{-1}X'y \quad (10)$$

of the trend parameters leads to empirical residuals $e = y - X\hat{\beta}_{OLS}$, and afterwards nonlinear least squares (NLS) is used to fit a parametric semi-variogram model $\gamma(h;\theta,\sigma,\alpha)$ to the empirical counterpart

$$\hat{\gamma}^{\#}(h) = \frac{1}{2|N(h)|}\sum_{N(h)}[e(s_i) - e(s_j)]^2$$
$$N(h) \equiv \{(s_i;s_j) : s_i - s_j = h; i,j = 1,\ldots,n\}. \quad (11)$$

Having obtained those prior variogram parameter estimates (θ,σ,α), one estimates the covariance matrix Σ and achieves a first GLS estimate

$$\hat{\beta}_{GLS} = (X'\hat{\Sigma}^{-1}X)^{-1}X'\hat{\Sigma}^{-1}y, \quad (12)$$

which allows for a new least squares fit of the variogram based on the residuals

$$y(s_i) - x'(s_i)\hat{\beta}_{GLS} \quad (13)$$

and a new $\hat{\Sigma}$ as the starting point of a new iteration. This iterative procedure is continued until a convergence criterion is met.

The dilemma with large data sets, such as the forest inventory data in this study, is that the high-dimensional $n \times n$ covariance matrix becomes intractable, and therefore GLS is not feasible. However, we will show that the first OLS fit can be sufficient under these circumstances. Therefore, OLS was applied to estimate the β parameters, and the variogram parameters were also derived from that single OLS fit.

Instead of Matheron's (1962) classical estimator, given above in Eq. (11), we used the robust variogram estimator

$$2\hat{\gamma}^{\#}(h) = \left(\frac{1}{|N(h)|}\sum_{N(h)}[e(s_i) - e(s_j)]^{1/2}\right)^4 \Big/ (0.457 + 0.494/|N(h)|), \quad (14)$$

proposed by Cressie and Hawkins (1980). Based on visual assessments of the resulting variogram range and having in mind the envisaged local kriging procedure, only location pairs having a distance smaller than h = 15 km were considered.

Site-index predictions are spatially kriged at any location s_0 in moving 100 point neighborhoods by

$$\hat{y}_0 = x(s_0)'\hat{\beta}_{OLS} + \hat{c}'_{\_}\hat{\Sigma}_{\_}^{-1}(y_{\_} - X_{\_}\hat{\beta}), \quad (15)$$

Here, "_" indicates the simplification of the universal kriging predictor in terms of a local predictor, and $\hat{\Sigma}_{\_}$ is no longer high-dimensional, but only 100 × 100 and thus numerically tractable.

Table 3
Information on the design of the applied B-spline regression functions for the mean model. In column *Knots* "P05" means a knot is placed at the 5th percentile of regressor variable. In column *Removed* it is indicated by "L2" that the two first columns are removed from X_z, a removal of the last two columns is indicated by "R2". "R3" in column *Summated* means that the last three columns are added up.

Variable	Unit	B-spline		Columns of X_z		Dimension of X_z
		Degree	Knots	Removed	Summated	
Total precipitation during the growing season	mm	3	0, P05, P50, P95, 5000	L2, R2		3
Total of average daily temperatures during the growing season	°C	3	0, P01, P05, P25, P50, P75, P95, P99, 6000	L2, R2		7
Elevation above sea level	m	2	0, 500, 800, 1100, 1500	L2		4
Stand age	years	3	0, 50, 100, 150, 251	L2	R3	3

For interval prediction, the universal kriging variance

$$\mathbb{E}(y_0-\hat{y}_0)^2=\sigma^2+\theta^2-c'\Sigma^{-1}c+[x(s_0)'-c'\Sigma^{-1}X]\times[X'\Sigma^{-1}X]^{-1}[x(s_0)'-c'\Sigma^{-1}X]' \quad (16)$$

was approximated by

$$\widehat{\mathbb{V}\mathrm{ar}}(\hat{y}_0)=\hat{\sigma}^2+\hat{\theta}^2-\hat{c}'_-\hat{\Sigma}_-^{-1}\hat{c}_-. \quad (17)$$

The rationale of omitting the rightmost additive term of Eq. (16) is that it quantifies the precision of the estimator of β, and we argue that the error of $\hat{\beta}$ can be neglected when using such large data sets, irrespective of whether GLS or OLS is applied.

Constructions of 95%-intervals were finally obatined by

$$\hat{y}_0\pm 1.96\sqrt{\widehat{\mathbb{V}\mathrm{ar}}(\hat{y}_0)}. \quad (18)$$

3.3. Modeling the mean function

Prior to the study, three conditions have been formulated, which had to be met by the mean function of the spatial site-index process given in Eq. (4); (i) linearity, to avoid iterative nonlinear least squares; (ii) flexibility, to model biologically plausible cause-and-effect curves of complex nonlinear relationships; (iii) parsimony, to allow for easy implementation of the entire model in Baden-Württemberg's forest inventory software. It is described in the following how these three conditions can be met using B-spline regression techniques.

A B-spline function is defined for the range of a vector of knots

$$\kappa=(\kappa_1,\ldots,\kappa_{l+1},\ldots,\ldots,\kappa_{d-l},\ldots,\kappa_d)^T, \quad (19)$$

and consists of d basis functions $\left(B_1^l(x),\ldots,B_d^l(x)\right)$ of degree l. Each of the basis functions is defined for the range between $l+2$ consecutive knots, and the definition range of a single basis function overlaps the definition ranges of $2l$ neighboring basis functions.

With given knot vector κ a basis function of degree $l=0$ is defined by

$$B_v^0=1_{[\kappa_v,\kappa_{v+1})}(x)=\begin{cases}1 & \text{for } \kappa_v\leqslant x<\kappa_{v+1}\\ 0 & \text{otherwise,}\end{cases}\qquad v=1,\ldots,d-1, \quad (20)$$

and according to de Boor (1972) and Cox (1972) basis functions of higher order are recursively defined by

$$B_v^l(x)=\frac{x-\kappa_v}{\kappa_{v+l}-\kappa_v}B_v^{l-1}(x)+\frac{\kappa_{v+l+1}-x}{\kappa_{v+l+1}-\kappa_{v+1}}B_{v+1}^{l-1}(x). \quad (21)$$

To guarantee that

$$\sum_{v=1}^{d}B_v^l(x)=1 \quad (22)$$

holds for every $x\in[\kappa_1,\kappa_d]$, the boundary knots are replicated l times, so that $\kappa_1=\cdots=\kappa_{l+1}$ and $\kappa_{d-l}=\cdots=\kappa_d$.

The entire regression matrix

$$X=(X_1,\ldots,X_p) \quad (23)$$

in Eq. (5) is composed of the p sub-matrices

$$X_z=\begin{pmatrix}B_1^l(x_{z1}) & \ldots & B_d^l(x_{z1})\\ \vdots & & \vdots\\ B_1^l(x_{zn}) & \ldots & B_d^l(x_{zn})\end{pmatrix}, \quad (24)$$

each of which corresponds to a single regressor variable $x_z=(x_{z1},\ldots,x_{zn})'$ with $z=1,\ldots,p$. This reveals that the B-spline regression technique is nothing else than a multiple linear regression model.

In this paper, B-spline basis functions of degree $l=3$ were generally used, except for elevation above sea level ([m]), where a degree of $l=2$ proved to be sufficient. It was found that relaxing the condition given in Eq. (22), in terms of adding up or removing some of the first or last columns of X_z (see Eq. (24)), has a stabilizing effect on the shape of the curves at the edges of the data range and also produces plausible shapes for extrapolations beyond that range. Detailed information on the chosen spline degrees and knot vectors, and of the design of the X_z matrices is given in Table 3.

3.4. Validation based on simulation of Gaussian random fields

A comprehensive validation is performed in terms of unbiasedness (i) of the NLS estimator of the variogram parameters, and (ii) of our approximation of the UK predictor (Eq. (15)). Furthermore, it is validated whether observed coverage rates obtained by Eq. (18), based on the approximation of the UK kriging variance given by Eq. (17), would be equal to the nominal 95% level.

Validations are based on simulations of Gaussian random fields (GRFs) on a lattice with grid cells of 100 m × 100 m width, which corresponds to the minimum mesh width applied in regional forest inventories. For simulations of GRFs the `R`-library `RandomFields` of Schlather (2001) was used. Because simulations with `RandomFields` did not work for the 100 m × 100 m grid covering the entire Baden-Württemberg region, a representative 90 km × 90 km sub-window W^* was constructed, which was arranged so that a broad range of site conditions is covered. As process parameters we used the parameter estimates from the complete data available for Norway spruce in Baden-Württemberg. The simulated lattice data were reduced to existing sample plot locations in W^* to take effects on the variogram estimation into account, which may arise from irregularly thinned sampling grids. To further examine the performance of the predictors presented in this paper the simulated data were split into training data and validation data (see B. below). The validation procedure comprises the following consecutive steps:

A. Obtain parameter estimates for simulation.
   1. Estimate β using OLS and the above described B-spline regression techniques for the Norway spruce data from the entire Baden-Württemberg region W and with PGS, TGS, elevation and stand age as covariates.
   2. Calculate residuals by $e = y - X\hat{\beta}_{OLS}$.
   3. Estimate the empirical semi-variogram (Eq. (14)) from the empirical residuals e.
   4. Estimate θ, σ and α of the exponential covariance function (Eq. (8)) using NLS for fitting the exponential semi-variogram model (Eq. (9)) to the empirical counterpart (Eq. (14)).
   5. Construct a 90 km × 90 km lattice in W^* with regular grid cells of 100 m × 100 m width.
   6. Obtain climatic covariates, elevation above sea level and stand age at the centroid locations of the lattice grid cells.
   7. Construct the design matrix X^* for the lattice data in W^* using the specifications of B-splines given in Table 3.
   8. Assume $X^*\hat{\beta}_{OLS}$ to be the true grid cell means in W^*.

B. Simulation: Perform as loop with 1000 runs.
   1. Simulate a realization of a Gaussian random field g^* with 0 mean and spatial covariance function $c(h|\hat{\theta}, \hat{\sigma}, \hat{\alpha})$ on the lattice in W^*.
   2. Calculate pseudo-data as $y^* = X^*\hat{\beta}_{OLS} + g^*$.
   3. Reduce pseudo-data to be available only at existing locations of forest inventory sample plots.
   4. Split the reduced pseudo-dataset into 90% model data y^*_M and 10% validation data y^*_V.
   5. Construct the design matrix X^*_M of the mean function for the model data.
   6. Apply OLS to estimate β from the model data $\hat{\beta}_M = (X^{*\prime}_M X^*_M)^{-1} X^{*\prime}_M y^*_M$.
   7. Calculate model residuals $e_M = y^*_M - X^*_M\hat{\beta}_M$.
   8. Use e_M to estimate the empirical variogram $\gamma^\sharp_M$.
   9. Estimate the parameters of the covariance function c_M by fitting an exponential variogram model to $\hat{\gamma}^\sharp_M$.
   10. Plug the estimates $\hat{\beta}_M$ and $\hat{c}_M$ in the UK kriging predictor (Eq. (15)), and perform local UK kriging with 100 neighbors at locations of the validation data.
   11. Plug the parameter estimates in the approximation of the UK kriging variance (Eq. (17)), and construct prediction intervals by Eq. (18).

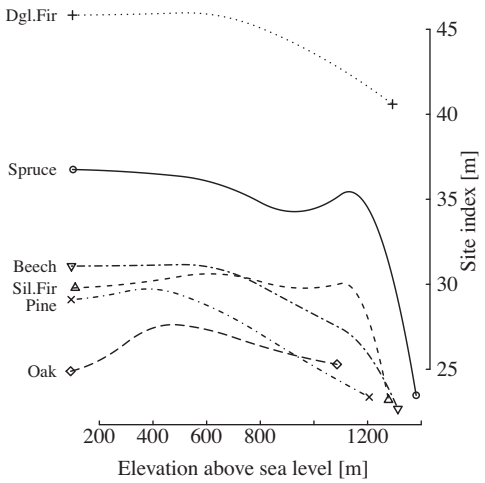

Fig. 2. Effect of elevation above sea level on site index modeled by B-spline basis functions, evaluated with other variables fixed at their sample means.

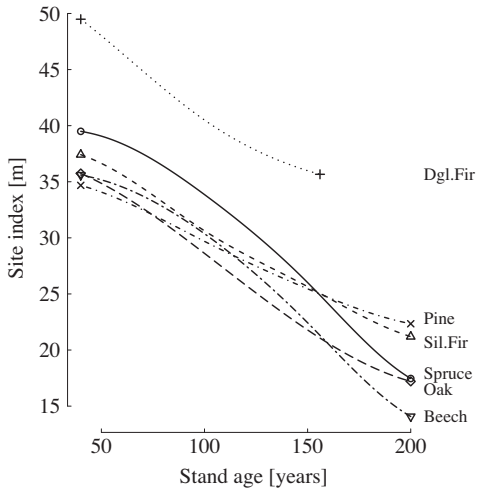

Fig. 3. Effect of stand age on site index modeled by B-spline basis functions, evaluated with other variables fixed at their sample means.

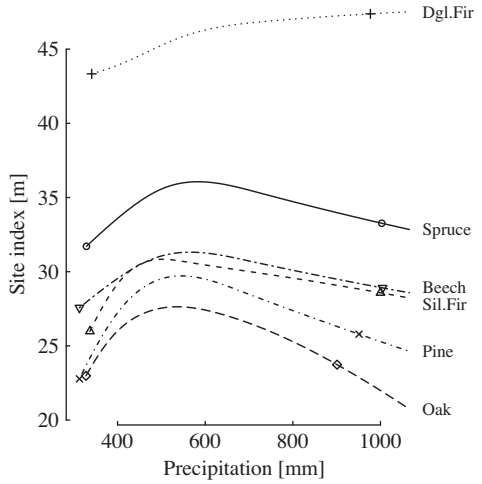

Fig. 4. Effect of total precipitation during the growing season (PGS) on site index modeled by B-spline basis functions, evaluated with other variables fixed at their sample means. The plot symbols indicate the range of the retrospective climate data.

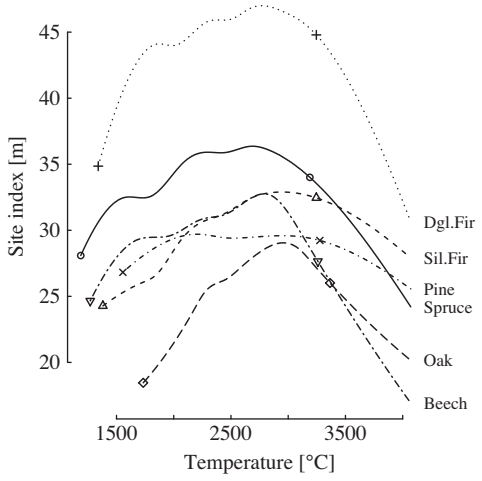

Fig. 5. Effect of total of average daily temperatures during the growing season (TGS) on site index modeled by B-spline basis functions, evaluated with other variables fixed at their sample means. The plot symbols indicate the range of the retrospective climate data.

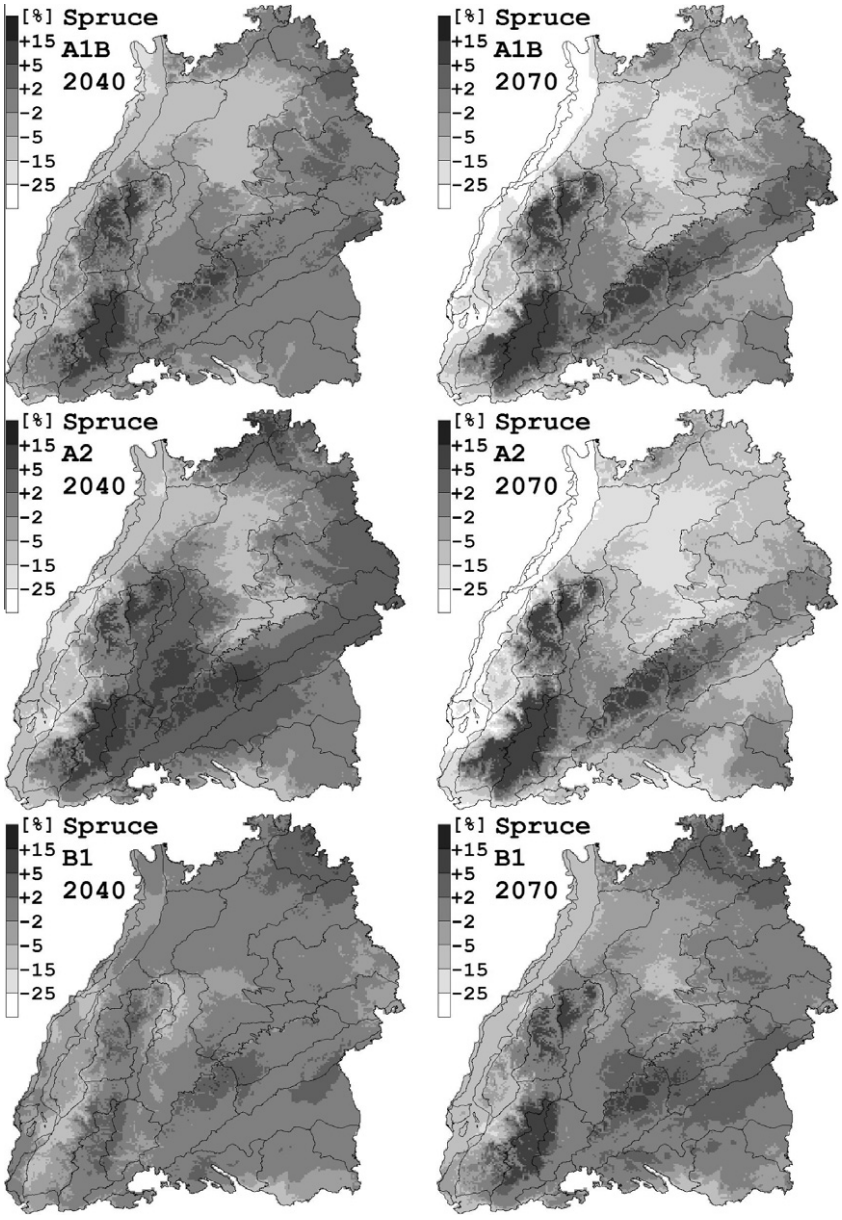

Fig. 6. Predicted relative changes of site index for Norway spruce until 2040 and 2070, covering IPCC SRES scenarios A1B, A2 and B1.

In each simulation run, the parameter estimates of the mean function and of the variogram model are returned, also the coverage rate of the interval predictor and the bias in terms of the difference between the mean of the simulated validation data and the mean of its predictions were calculated.

4. Results

4.1. Mean effects

The estimated effect which a certain independent variable has on site index is shown by varying one variable at a time and holding other variables constant at their means derived from the model data set. The variable elevation above sea level was used as proxy variable which captures variance unexplained by the climate variables; a possible hidden effect may be the influence of wind speed, which may lead to lower site indexes with increasing elevation above sea level, as wind speed usually increases with increasing elevation. As expected, for all tree species except oak site index shows a more or less clear decreasing trend with increasing elevation above sea level (Fig. 2). The B-spline fits for Norway spruce and common beech have distinct peaks at about 1100 m above sea level. This phenomenon is caused by highly productive sites in relatively high elevation areas of southern Schwarzwald mountains nearby the Schluchsee lake, where follow-up measurements of forest inventories have revealed high periodical increments of growing stock. However, this causes no problems for predictions in other regions, since an elevation above sea level higher than 1100 m occurs almost exclusively in the above mentioned region, except for one single mountain peak in Northern Schwarzwald, the Hornisgrinde, which has 1164 m elevation.

Keeping other variables fixed, site index shows a clearly decreasing trend with increasing stand age (Fig. 3). This is due to two well-known effects. Since highly productive forests are generally managed in short rotation times, old stands rather grow on poor sites and have therefore lower site indexes; and in relation to their short lifetime, younger forest stands were more able to

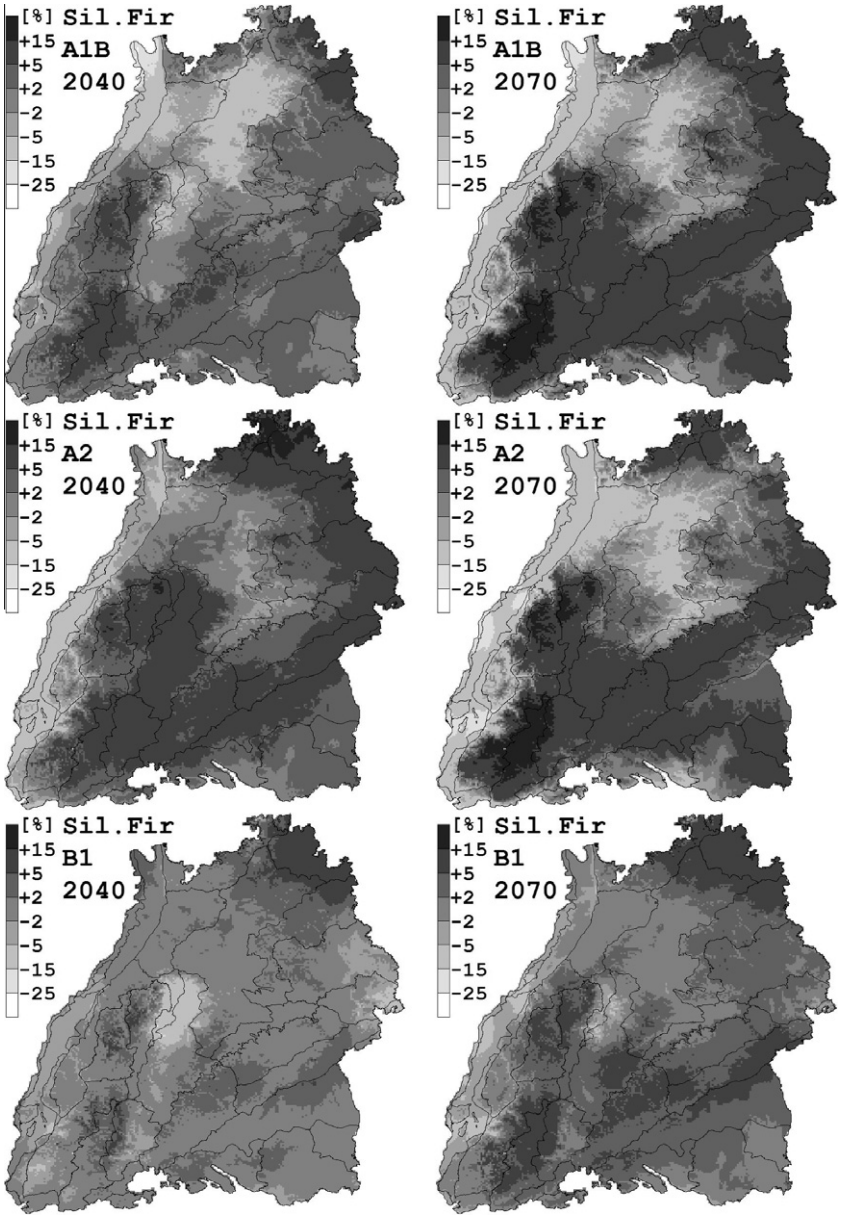

Fig. 7. Predicted relative changes of site index for silver fir until 2040 and 2070, covering IPCC SRES scenarios A1B, A2 and B1.

benefit from positive effects caused by increased atmospheric deposition of nitrogen and sulfur in the past. That implies that, with respect to site index, younger forest stands might react more sensitive to a changing climate. Because atmospheric deposition data were not available for the present study, the variable stand age is used as additional proxy variable to account for so far unknown effects correlated with stand age. By setting the proxy variable stand age to a constant value of 100 years, when using the model for spatio-temporal predictions of site index, it is assumed that likewise the unknown effects are consecutively fixed at a constant level.

Among the six tree species, only site index of Douglas-fir continuously increases with increasing PGS (Fig. 4). For the other tree species an optimum is presumably achieved between 500 mm and 600 mm. While for sessile/common oak and Scots pine site index decreases quite rapidly for PGS higher than the optimal supply, site index of silver fir, common beech and Norway spruce declines rather moderately beyond the optimum PGS.

The curves in the Figs. 2–5 were plotted for the entire range covering both types of data sets, the retrospective climate data and the projection data from all IPCC SRES scenarios. To judge whether predictions might become uncertain by extrapolations, the range of the retrospective data is indicated by species dependent plot symbols. Whereas for PGS the retrospective model data cover most of the projection data range, the TGS projections go farther beyond the maximum of the retrospective TGS data, particularly resulting from IPCC SRES scenarios A1B and A2. Similar to the B-splines for the PGS, the curves for TGS show also nearly a parabolic shape with a distinct optimum for most tree species (Fig. 5). However, in contrast to the other tree species, site index of Scots pine has a wide optimum range for TGS. Furthermore, site index of Scots pine declines less rapidly at the edges of the data range. Similar to Scots pine site index of silver fir decreases quite moderately with further increase of high TGS.

4.2. Site-index predictions

The results of the spatio-temporal predictions are presented as maps in Figs. 6–11, in which the spatio-temporal changes of site index are expressed as percentage changes with respect to the

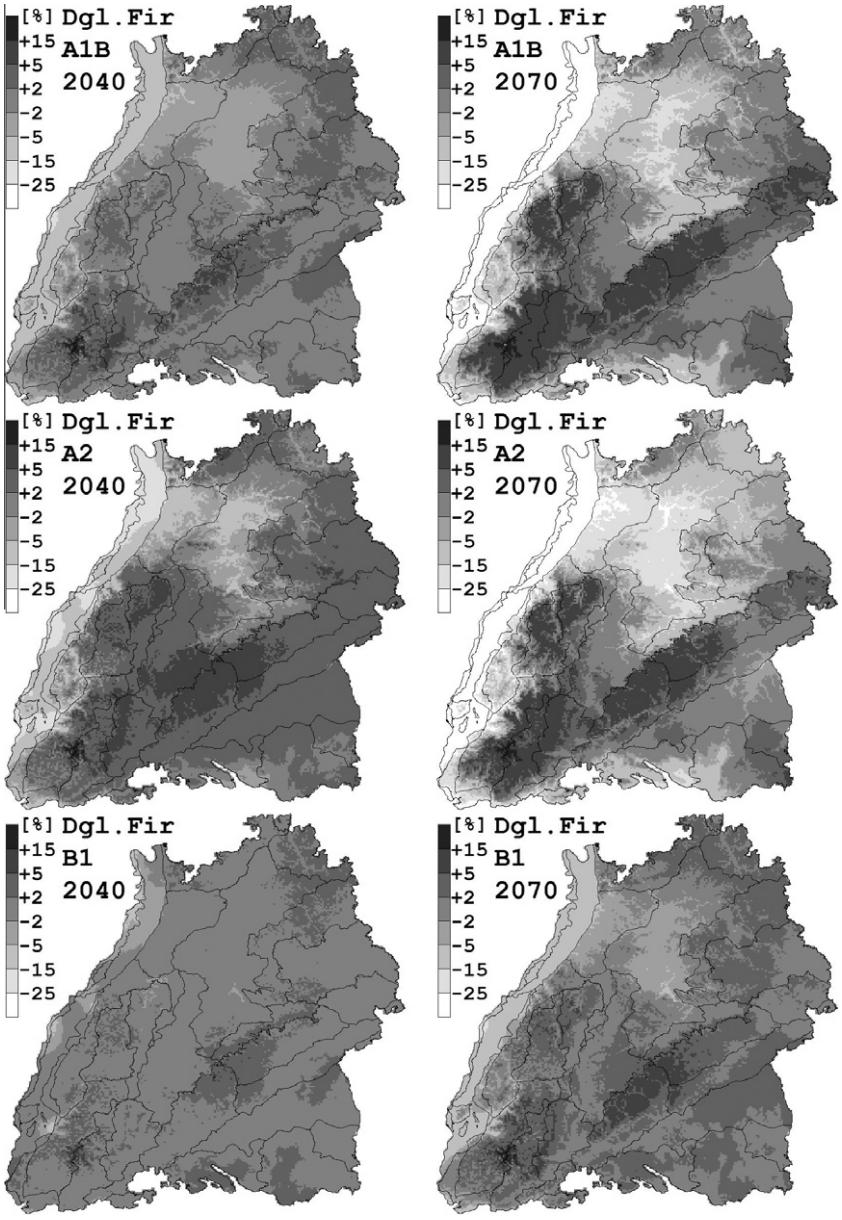

Fig. 8. Predicted relative changes of site index for Douglas-fir until 2040 and 2070, covering IPCC SRES scenarios A1B, A2 and B1.

reference year 2007. For this purpose, site-index predictions were calculated based on 30-year averages of climate variables for the two periods [2011,...,2040] and [2041,...,2070] and presented as relative changes compared to the corresponding site index in 2007.

For all of the three IPCC SRES scenarios only minor changes of site index are predicted until 2040 for Norway spruce on the currently highly productive sites of the Alpine foothills region. Whereas site index also remains nearly unchanged in Neckarland, Kraichgau and Rhine valley until 2040 based on the conservative scenario B1, a decrease is predicted in these regions when using climate projection data from scenarios A1B and A2. Site index of Norway spruce will presumably increase in high elevation mountainous regions of Schwarzwald and Swabian Alps, in relative weak expression for scenario B1 and more clearly for A1B and A2. When using subsequent climate projections from REMO model until 2070, the observed trends from predictions until 2040 will be further strengthened. That is site index will decrease in Rhine valley, Kraichgau and Neckarland, not only for scenarios A1B and A2, but also for B1; and site index will increase in Schwarzwald and Swabian Alps.

Site-index predictions of silver fir for scenarios A1B and A2 and until 2040 indicate a decreasing trend in Rhine valley, Kraichgau and Neckarland, and an increasing trend in Schwarzwald and in Swabian Alps. However, in comparison to Norway spruce the site index of silver fir will also increase on larger areas of lower elevation mountainous regions. According to scenario A2 site index of silver fir will additionally increase until 2040 in Tauberland and in the Schwäbisch-Fränkischer Wald, and in these regions even more clearly until year 2070 for both scenarios A1B and A2. In contrast to Norway spruce, for which predictions based on scenarios A1B and A2 show that site index remains nearly constant until 2070 in the Alpine foothills region, a moderate increase on those sites may occur for silver fir.

When applying scenario B1 until 2040, almost no changes in site index of Douglas-fir may occur in relation to reference year 2007; and until 2070 scenario B1 leads to slightly decreased site index in Rhine valley, Kraichgau and Neckarland. In the same geographical regions predictions with scenario A2 until 2040 and with A1B until 2070 result in decreasing site indexes. Based on climate projections using scenarios A1B and A2 and until 2070 site

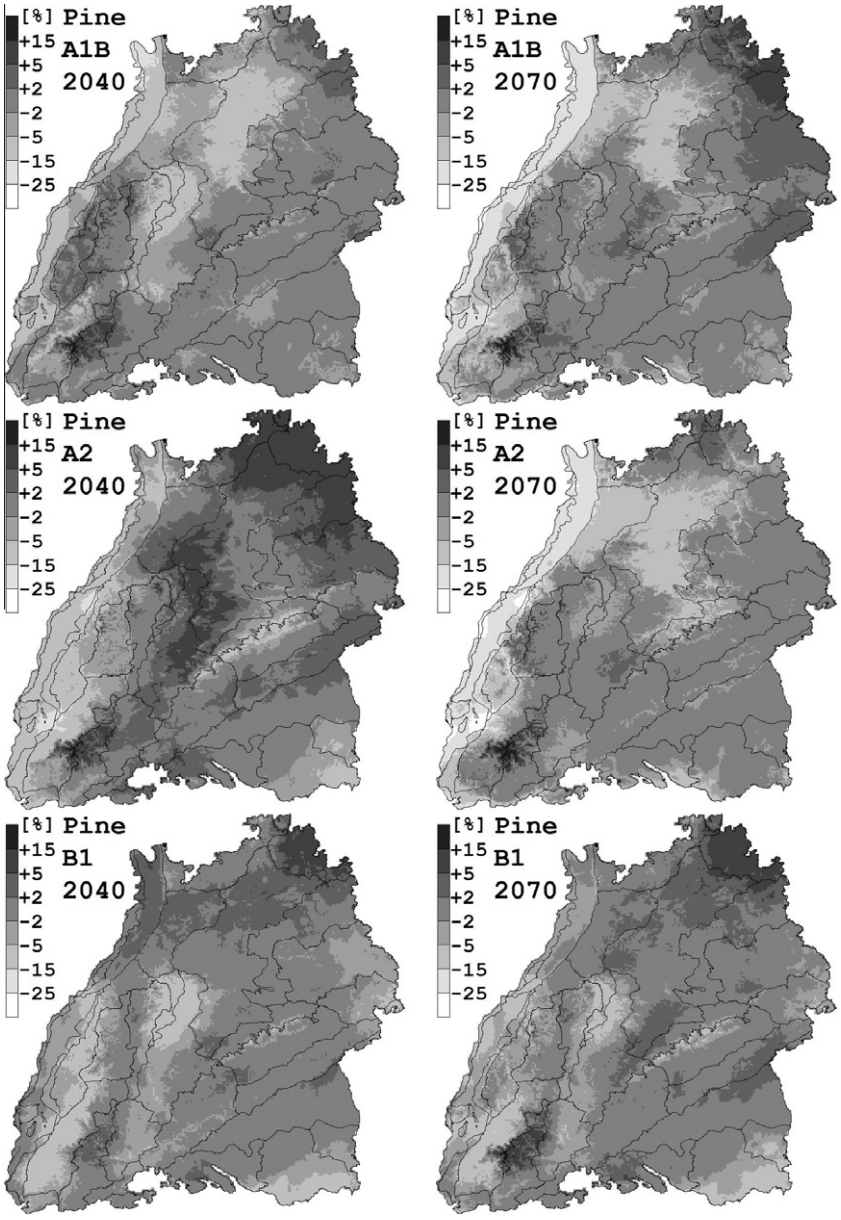

Fig. 9. Predicted relative changes of site index for Scots pine until 2040 and 2070, covering IPCC SRES scenarios A1B, A2 and B1.

index of Douglas-fir may only increase in high elevation areas of Schwarzwald and Swabian Alps.

Site index of Scots pine decreases in Rhine valley for scenarios A1B and A2 and also in Schwarzwald mountains for scenario A2. Scots pine's site index might increase in Tauberland, in the Schwäbisch-Fränkischer Wald, in Gäu region and on Baar sites, more obviously for scenario A2 than for A1B. With scenario B1 site index remains nearly unchanged in Baden-Württemberg region, except for Tauberland region, where an increase may occur. For the climate projection data applied in the present study, Scots pine's site index generally alters less than site index of the other conifers examined here.

Using scenarios A2 and A1B until 2070, site index of sessile oak and common oak decreases in Kraichgau and Neckarland and more strongly in Rhine valley. In almost every other region site index of oak increases, especially in Schwarzwald, Baar and Swabian Alps for scenarios A1B and B2, and also quite clearly for scenario B1.

Predicted changes of site index for common beech show nearly the same spatial patterns as for Norway spruce. However, in comparison to Norway spruce site index of common beech may increase on larger areas with lower elevation of Schwarzwald and Swabian Alps. Additionally, site index of common beech increases in the south-eastern part of the Alpine foothills region for scenarios A1B and B2 until 2070 and for B1 in Schwäbisch-Fränkischer Wald, whereas site index of Norway spruce remains almost unchanged on those sites with respect to the same conditions.

4.3. Validation results

By means of 1000 simulations of Gaussian random fields in a 90 km $\times$ 90 km sub-region of entire Baden-Württemberg, the performance of the OLS parameter estimator of the mean function, of the NLS parameter estimator of the variogram model, as well as of the proposed approximation of the UK predictor and of the corresponding interval predictor is assessed. The simulation study clearly states that the mean parameter estimates obtained by the OLS estimator for the 17 B-spline basis functions are close to the true values, what must be expected from theory. The relative bias for the 17 parameters ranges from -2.1% to 2.0% and is therefore negligibly small.

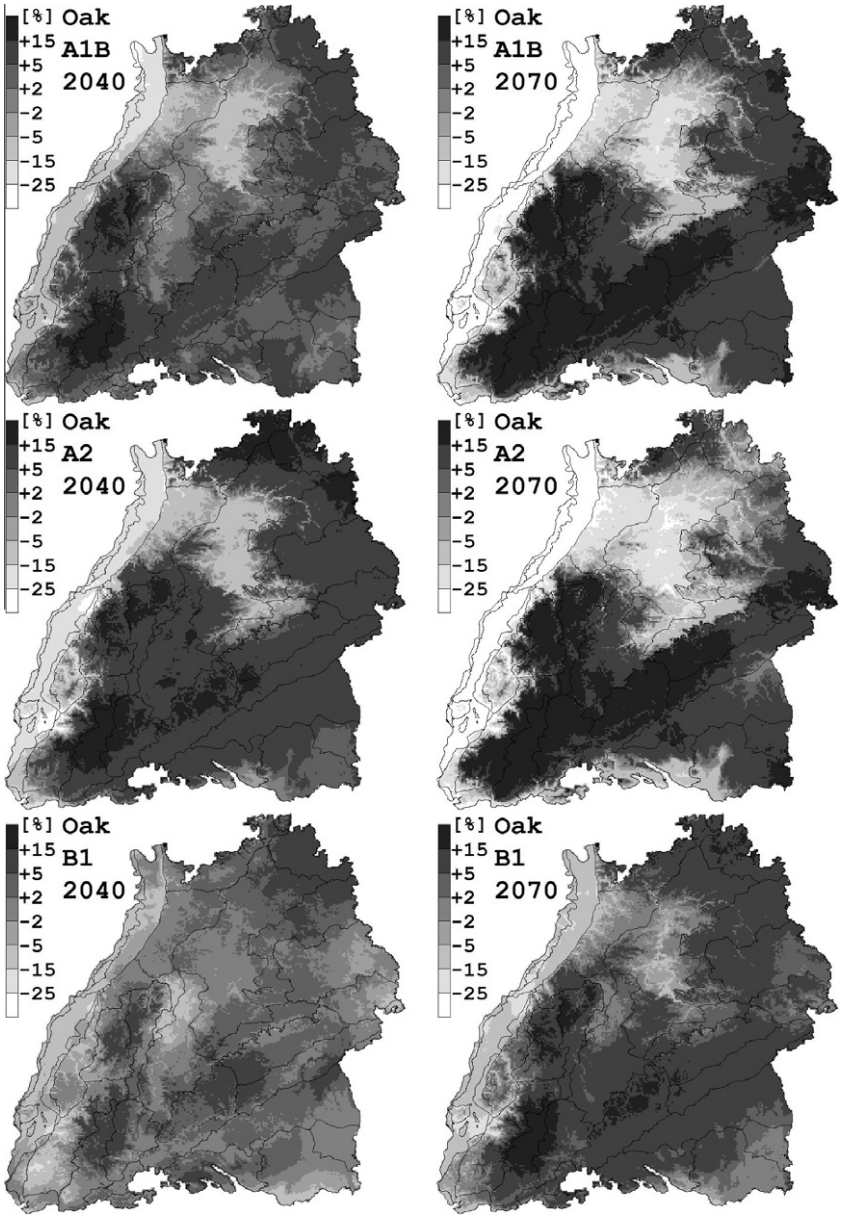

Fig. 10. Predicted relative changes of site index for sessile/common oak until 2040 and 2070, covering IPCC SRES scenarios A1B, A2 and B1.

The true semi-variogram is completely covered by the 95% envelope obtained from 1000 semi-variogram estimates (see Fig. 12), each of which is fitted using residuals obtained from predictions by the mean function with parameters estimated via OLS. Furthermore, the mean of the semi-variogram estimates from 1000 GRF simulations is almost of same shape as the true semi-variogram. The true practical range parameter of the exponential semi-variogram model, which is $3\alpha = 8469$ (Eq. (9)), differs only slightly from the corresponding posterior mean 7664. Thus, the NLS estimator of the parametric semi-variogram model based on the OLS residuals is absolutely sufficient, and one can proceed without the computationally more demanding iterative fittings of the mean and the variogram model.

The linear mean functions and the variogram models were estimated by means of the simulated data at real inventory locations. For the purpose of validation, in each of the 1000 simulations 10% of the data were randomly excluded from model fitting. The bias of the proposed approximation (Eq. (15)) of the universal kriging predictor is assessed in terms of the average difference between the predictions and the simulations at the validation locations. The relative bias of the 1000 simulations ranges from −1.1% to 1.0% (see Fig. 13), and the average bias is −0.0027%. Hence, the approximation of the UK predictor, presented in Eq. (15), proves to be approximately unbiased under the given test conditions.

The applied interval predictor (Eq. (18)) based on the approximation of the kriging variance (Eq. (16)) shown in Eq. (17) achieves coverage rates ranging from 0.925% to 0.971% (see Fig. 14). The mean coverage rate from 1000 simulations is 0.94951%, which is very close to the nominal probability of 95%. That means the proposed interval predictor is sufficiently exact.

Summarizing, the methods proposed in this paper comprise (i) an approximately unbiased spatial predictor of site index in Baden-Württemberg, (ii) an unbiased interval predictor of site index, and (iii) an approximately unbiased NLS estimator of the spatial covariance function.

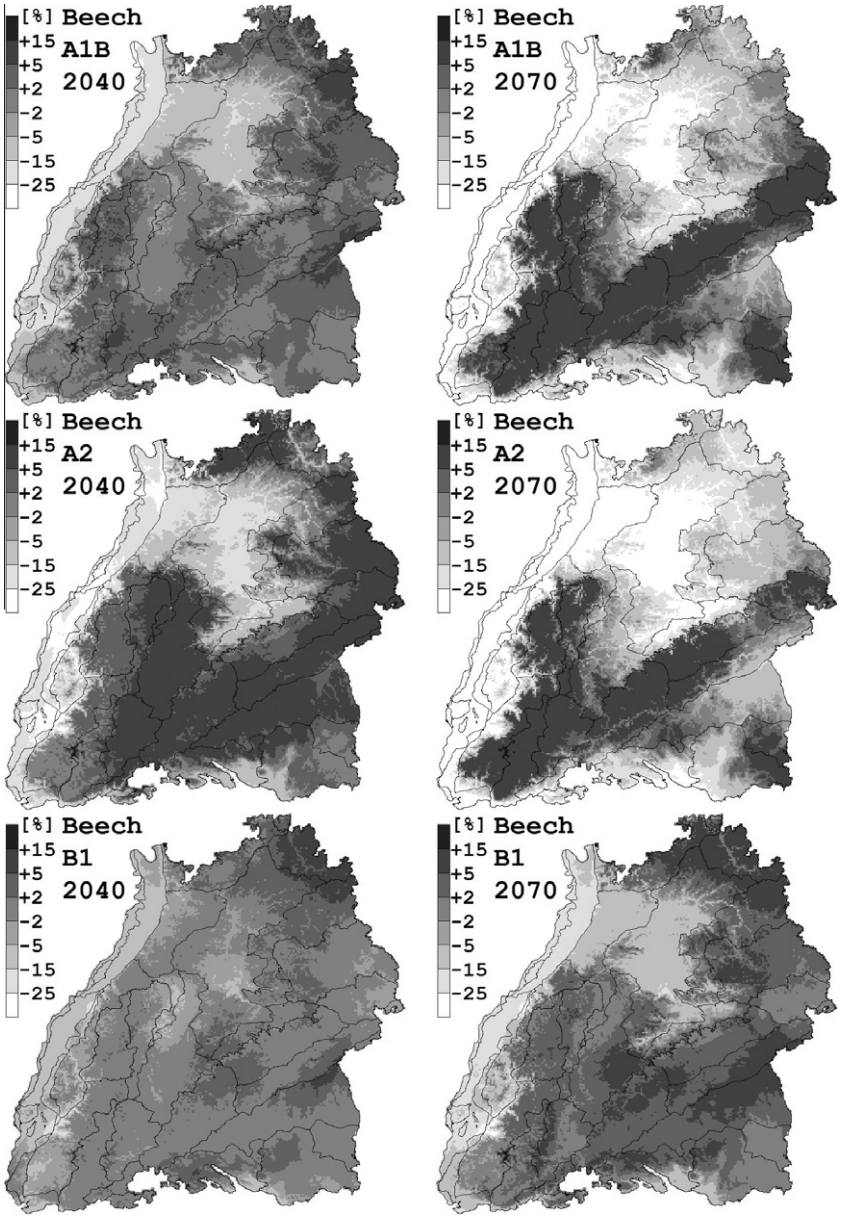

Fig. 11. Predicted relative changes of site index for common beech until 2040 and 2070, covering IPCC SRES scenarios A1B, A2 and B1.

5. Discussion and conclusions

This paper provides a straight forward and numerically easy to apply methodological framework for spatio-temporal site-index prediction based on a flexible and simplified universal kriging method and on a large amount of representatively distributed forest inventory sample plots. Using B-spline basis functions with only a small number of knots enables application of OLS for linear models and produces flexible cause-and-effect curves having a biologically plausible shape. To decide upon an optimal number and location of knots, modern standard software packages, such as the R-library `mgcv` (Wood, 2000), work with penalized least squares based on minimization of second order derivatives; for details the reader is referred to the standard textbooks of Wood (2000) and Hastie and Tibshirani (1996). However, in this study we chose the number and location of the knots heuristically, guided by visual assessments, to avoid illogical behavior of the smooth functions beyond the range of the model data. That was essential, because the regression model was applied to climate projection data which exceed the range of the model data, meaning that the trend model had to be extrapolated in some situations. Furthermore, we could reduce the usually extremely large number of regression parameters of nonparametric models to only 17 in our linear UK trend model, which thus can easily be implemented in the stand-alone forest inventory software of Baden-Württemberg.

The reader should note that the UK approach presented in this paper also belongs to the broad class of geoadditive models according to modern terminology used in the German standard textbook on regression modeling of Fahrmeir et al. (2009). In Fahrmeir et al. (2009) applications are shown, where statistical inference is based on penalized least squares or likelihood approaches, a mixed model representation, or the full Bayesian inference with application of Markov chain Monte Carlo (MCMC)

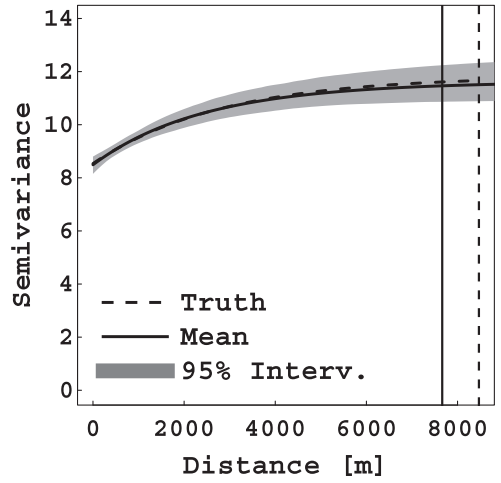

Fig. 12. Mean and 95% envelope of exponential semi-variogram estimates obtained by least squares fits to empirical semi-variograms resulting from residuals of mean curve predictions based on 1000 simulations of Gaussian random fields.

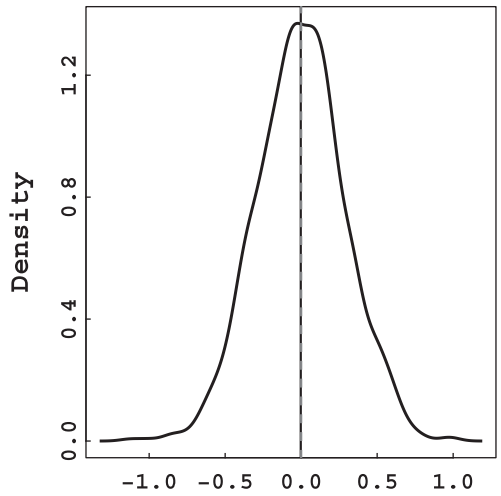

Fig. 13. Distribution of relative bias [%] of the universal kriging predictor. For each of the 1000 Gaussian random field simulations, bias was evaluated on the 10% validation data, which were excluded from model fitting. The vertical solid line indicates mean relative bias from the 1000 simulations.

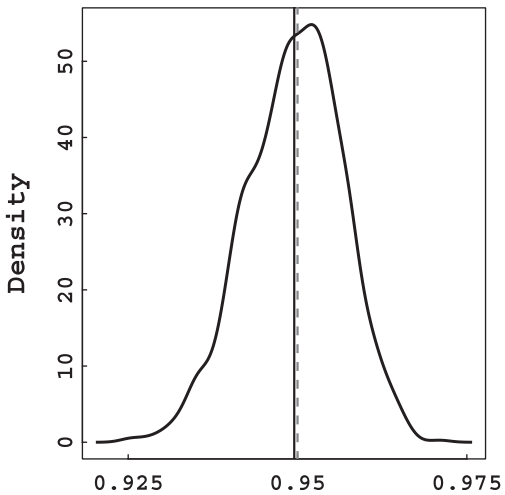

Fig. 14. Distribution of coverage rates of the interval predictor. For each of the 1000 Gaussian random field simulations, coverage rate was evaluated on the 10% validation data, which were excluded from model fitting. The vertical solid line indicates mean coverage rate from the 1000 simulations.

techniques. Bayesian inference using MCMC is often applied for discrete location variables on Markov random fields and when data are sparse. However, in the application presented in this paper, the location variables are continuous x- and y-coordinates, and consequently the theory of Gaussian random fields was applied. Due to the large amount of data a representation of our regression problem in form of a mixed model had failed, but it is shown that easy to apply ordinary least squares techniques may also provide an unbiased point predictor and an almost exact interval predictor if large data sets are available.

The approach to spatial interpolation presented in this paper is in contrast to the methods shown in Wood (2006) for smooth modeling of spatial effects using tensor product splines or thin plate regression splines. Whereas the latter methods are hard to implement in stand-alone software programs, our approach is based on a parsimonious spatial covariance function having only three parameters and resulting in the straightforward and easy to apply spatial predictor in Eq. (15).

In fact, the extrapolations beyond the range of modeling data may be seriously misleading. However, this is a general dilemma associated with the prediction of climate change effects, particularly when dealing with long-term projections of climate variables which are outside the range of the climate conditions known from the past. Future attempts to solve that dilemma must make use of additional inventory data from other regions and countries, where more extreme climate conditions than in Baden-Württemberg can be observed.

All unknown effects on site index were covered by the spatially structured error which is modeled by the exponential covariance function; in this context the reader may recall the mixed-model representation of the universal kriging model in Eq. (5) with b being the spatial random effect. So far, no information was available for soil conditions in Baden-Württemberg. Therefore, in future work a hydrologic balance model will be applied to the retrospective climate data as well as to the climate projection data, and the model output will be used as additional regressor in the UK trend function. The same applies to nitrogen and sulfur, for which no reliable temporal and spatial data of atmospheric depositions were available. According to the findings in Albert and Schmidt (2010), CO2 concentration was not used as regressor. The latter authors found that site index is linearly related to atmospheric CO2 concentration in the past, but when using future prognoses of CO2 from IPCC SRES scenarios the projections of site index showed ill performance.

Ideally, the growth pattern should have been observed over long periods to model dominant height growth for projections of site index (Assmann, 1970). That means our approach, by fitting the growth model to height increments obtained from inventory data and applying Eq. (3) for height growth projections, does not exactly yield site index. However, the authors are aware of the fact that the approach of height projection applied in this study is rather an approximation, due to the lack of long-term observations, which have not been available. One could also imagine using the year of germination as an additional proxy to account for changing growth conditions, which may possibly be caused by increased atmospheric deposition of nitrogen and sulfur in the past. However, since the inventory data were collected only over a short time period, the year of germination is closely represented by the variable stand age from our model. As a possible solution in future studies, additional data from long-term trial plots could be pooled together with the already applied inventory data to more precisely account for growth trends over time. Future periodic inventories could also stepwise be integrated to improve the model.

The parabolic shape of the PGS regression curves seems arguable, as for higher precipitation enhanced water availability is generally expected. Because soil variables, such as nutrient supply or

water holding capacity, were not available for the present study, the B-spline curves may also represent other unknown effects associated with PGS. Keeping other variables fixed, high precipitation generally hinders soil aeration and promotes acidification, which both may lead to reduced nutrient supply and finally to a lower site index.

The approach presented in this paper to derive retrospective climate data is rather complex and computational demanding, especially with respect to the dynamical downscaling steps incorporating the NCAR/NCEP reanalysis series and using the regional climate model WRF. The reader may ask whether just a regionalization of long-term met station observations would likewise provide sufficient results. The rationale for our approach was to consistently apply process-based climate model data for both, the prediction and the modeling of site index. Another reason was that met stations are generally installed at locations showing homogeneous topographical conditions, and thus making a downscaling solely based on regression analysis nearly impossible.

Major results from IPCC SRES scenarios are predictions of future greenhouse gas emissions. However, at present we have ignored the possible effects on tree growth caused by an increase of atmospheric CO2 concentration. Higher supply of CO2 may lead to higher absolute photosynthesis rates and enhanced water efficiency. Both effects may partially compensate for depressing effects induced by drought as found in the papers of Tolley and Strain (1984) and Aber et al. (1995). In future work a collaboration with plant physiologists is planned, to consider state-of-the-art knowledge about these mechanisms.

In the present study, the spatial autocorrelation is assumed to be time-invariant, meaning that θ and α in Eq. (8) remain constant over time. The authors are aware of the fact that this might not hold. However, in Baden-Württemberg regional forest inventories with relatively dense sampling grids have regularly been conducted not until the late nineties, and from most of the sample plots only one follow-up measurement is available because of the 10 year inventory cycle. Thus, the available inventory data were not sufficient to model temporal effects on the spatial error component explicitly.

The reader may have expected envelopes for the predicted future changes of site index. In the present paper the relative differences are shown between site-index predictions for a certain future period and for the reference year 2007 (Figs. 6–11). The spatially correlated error (right summand in Eq. (15)) of the mean function is held constant over time. Thus, when calculating the difference between the two site index predictions at a single location, the predicted spatially correlated error cancels out. Additionally, the error of the mean model can be neglected when spatially predicting site index; this is due to the large amount of data. Because the error of the mean model can be neglected, and because spatial error is constant over time, a reasonable approach to model uncertainty of future site index predictions is to apply different climate scenarios. Therefore, in future work, projections of different regional climate models will be used, not only for the well-known IPCC SRES scenarios, but also for scenarios expected in the near future based on the Representative Concentration Pathways (RCP) (Moss et al., 2010).

References

Aber, J.D., Ollinger, S.V., Federer, C.A., Reich, P.B., Goulden, M.L., Kicklighter, D.W., Melillo, J.M., Lathrop Jr., R.G., 1995. Predicting the effects of climate change on water yield and forest production in the northeastern United States. Climate Res. 5 (3), 207–222.

Albert, M., Schmidt, M., 2010. Climate-sensitive modelling of site-productivity relationships for Norway spruce (*Picea abies* (L.) Karst.) and common beech (*Fagus sylvatica* L.). Forest Ecol. Manag. 259 (4), 739–749.

Assmann, E., 1970. The Principles of Forest Yield Study. Pergamon Press.

de Boor, C., 1972. On calculating with B-splines. J. Approx. Theory 6, 50–62.

Böhner, J., 2006. General climatic controls and topoclimatic variations in Central and High Asia. Boreas 35 (2), 279–295.

Böhner, J., Antonić, O., 2008. Land-surface parameters specific to topo-climatology. Dev. Econ. 33, 195–226.

Chmielewski, F.M., Rötzer, T., 2001. Response of tree phenology to climate change across Europe. Agr. Forest Meteorol. 108 (2), 101–112.

Cox, M.G., 1972. The numerical evaluation of B-splines. IMA J. Appl. Math. 10 (2), 134–149.

Cressie, N.A.C., 1991. Statistics for Spatial Data. John Wiley & Sons.

Cressie, N., Hawkins, D.M., 1980. Robust estimation of the variogram. J. Int. Ass. Math. Geol. 12, 115–125.

Ellenberg, H., 2009. Vegetation Ecology of Central Europe. Cambridge University Press.

Fahrmeir, L., Kneib, T., Lang, S., 2009. Regression. Springer, In German.

Hastie, T.J., Tibshirani, R.J., 1996. Generalized Additive Models. Chapman & Hall/CRC.

Iverson, L.R., Prasad, A.M., 1998. Predicting abundance of 80 tree species following climate change in the eastern United States. Ecol. Monogr. 68 (4), 465–485.

Iverson, L.R., Prasad, A.M., 2000. Potential changes in tree species richness and forest community types following climate change. Ecosystems 4 (3), 186–199.

Jacob, D., Andrae, U., Elgered, G., Fortelius, C., Graham, L.P., Jackson, S.D., Karstens, U., Koepken, C., Lindau, R., Podzun, R., Rockel, B., Rubel, F., Sass, H.B., Smith, R.N.D., Van den Hurk, B.J.J.M., Yang, X., 2001. A comprehensive model intercomparison study investigating the water budget during the BALTEX-PIDCAP period. Meteorol. Atmos. Phys. 77 (1–4), 19–43.

Jacob, D., 2001. A note to the simulation of the annual and inter-annual variability of the water budget over the Baltic Sea drainage basin. Meteorol. Atmos. Phys. 77 (1–4), 61–73.

Kahn, M., 1995. Quasikausale Modellierung des Standort-Leistungs-Bezuges als Voraussetzung zum Aufbau flexibler Mischbestandsmodelle – Modelling site dependent height growth as a basis for the design of growth simulators for uneven-aged mixed species stands. Forstwiss. Centralbl. 114, 175–187, In German with English summary.

Kalnay, E., Kanamitsu, M., Kistler, R., Collins, W., Deaven, D., Gandin, L., Iredell, M., Saha, S., White, G., Woollen, J., Zhu, Y., Leetmaa, A., Reynolds, R., Chelliah, M., Ebisuzaki, W., Higgins, W., Janowiak, J., Mo, K.C., Ropelewski, C., Wang, J., Jenne, R., Joseph, D., 1996. The NCEP/NCAR 40-year reanalysis project. B. Am. Meteorol. Soc. 77 (3), 437–471.

Köhl, M., Hildebrandt, R., Olschofsky, K., Köhler, R., Rötzer, T., Mette, T., Pretzsch, H., Köthe, M., Dieter, M., Abiy, M.A., Makeschin, F., Kenter, B., 2010. Combating the effects of climatic change on forests by mitigation strategies. Carbon Balance Manag. 5 (8).

Langkamp, T., Böhner, J., 2011. Influence of the compiler on multi-CPU performance of WRFv3. Geosci. Model Dev. 4 (3), 611–623.

Latta, G., Temesgen, H., Adams, D., Barrett, T., 2010. Analysis of potential impacts of climate change on forests of the United States Pacific Northwest. Forest Ecol. Manag. 259 (4), 720–729.

Lindner, M., Maroschek, M., Netherer, S., Kremer, A., Barbati, A., Garcia-Gonzalo, J., Seidl, R., Delzon, S., Corona, P., Kolström, M., Lexer, M.J., Marchetti, M., 2000. Climate change impacts, adaptive capacity, and vulnerability of European forest ecosystems. Forest Ecol. Manag. 259 (4), 698–709.

Majewski, D., 1991. The Europa-Modell of the Deutscher Wetterdienst. In: Proceedings of the ECMWF Seminar on Numerical Methods in Atmospheric Models, vol. 2, pp. 147–191.

Mandallaz, D., 1993. Geostatistical methods for double sampling schemes: application to combined forest inventories. Habilitation-Thesis, Swiss Federal Institute of Technology (ETH).

Matheron, G., 1962. Traite de Geostatistique Appliquee. Memoires du Bureau de Recherches Geologiques et Minieres, No. 14. Editions Technip, Paris.

Menzel, A., Fabian, P., 1999. Growing season extended in Europe. Nature 397, 659-659.

Moss, R.H., Edmonds, J.A., Hibbard, K.A., Manning, M.R., Rose, S.K., van Vuuren, D.P., Carter, T.R., Emori, S., Kainuma, M., Kram, T., Meehl, G.A., Mitchell, J.F.B., Nakicenovic, N., Riahi, K., Smith, S.J., Stouffer, R.J., Thomson, A.M., Weyant, J.P., Wilbanks, T.J., 2010. The next generation of scenarios for climate change research and assessment. Nature 463, 747–756.

Nakicenovic, N., Alcamo, J., Davis, G., de Vries, B., Fenhann, J., Gaffin, S., Gregory, K., Grubler, A., Jung, T.Y., Kram, T., La Rovere, E.L., Michaelis, L., Mori, S., Morita, T., Pepper, W., Pitcher, H.M., Price, L., Riahi, K., Roehrl, A., Rogner, H.-H., Sankovski, A., Schlesinger, M., Shukla, P., Smith, S.J., Swart, R., van Rooijen, S., Victor, N., Dadi, Z., 2000. Emissions Scenarios. A Special Report of IPCC Working Group III. Pacific Northwest National Laboratory, Richland, WA (US), Environmental Molecular Sciences Laboratory (US).

Neuman, S.P., Jacobson, E.A., 1984. Analysis of nonintrinsic spatial variability by residual kriging with application to regional groundwater levels. J. Int. Ass. Math. Geol. 16, 499–521.

Nothdurft, A., Kublin, E., Lappi, J., 2006. A non-linear hierarchical mixed model to describe tree height growth. Eur. J. For. Res. 125 (3), 281–289.

Roeckner, E., Bäuml, G., Bonaventura, L., Brokopf, R., Esch, M., Giorgetta, M., Hagemann, S., Kirchner, I., Kornblueh, L., Manzini, E., Rhodin, A., Schlese, U., Schulzweida, U., Tompkins, A., 2003. The atmospheric general circulation model ECHAM-5: model description. Report No. 349, Max-Planck-Institute of Meteorology. Hamburg, Germany.

Roeckner, E., Arpe, K., Bengtsson, L., Christoph, M., Claussen, M., Dümenil, L., Esch, M., Giorgetta, M., Schlese, U., Schulzweida, U., 1996. The atmospheric general circulation model ECHAM-4: Model description and simulation of the present

day climate. Report No. 218, Max-Planck-Institute of Meteorology. Hamburg, Germany.
Schabenberger, O., Gotway, C.A., 2005. Statistical Methods for Spatial Data Analysis. Chapmann & Hall/CRC.
Schlather, M., 2001. Simulation of stationary and isotropic random fields. R-News 1 (2), 18–20.
Skamarock, W.C., Klemp, J.B., Dudhia, J., Gill, D.O., Barker, D.M., Wang, W., Powers, J.G., 2005. A description of the Advanced Research WRF Version 2. NCAR Technical Note NCAR/TN-468+STR.
Sloboda, B., 1971. Zur Darstellung von Wachstumsprozessen mit Hilfe von Differentialgleichungen erster Ordnung – On the description of growth processes with first order differential equations. Dissertation-Thesis, Univ. Freiburg. (In German).
Tolley, L.C., Strain, B.R., 1984. Effects of CO2 enrichment and water stress on growth of Liquidambar styraciflua and Pinus taeda seedlings. Can. J. Botany 62 (10), 2135–2139.
v.Wilpert, K., 1990. Die Jahrringstruktur von Fichten in Abhängigkeit vom Bodenwasserhaushalt auf Pseudogley und Parabraunerde: Ein Methodenkonzept zur Erfassung standortsspezifischer Wasserstressdisposition – The year ring structure of spruce trees dependent on soil moisture of pseudogley and leached brown soil sites. Dissertation-Thesis, Univ. Freiburg. (In German).
Wood, S.M., 2006. Generalized Additive Models: An Introduction with R. Chapman & Hall/CRC.
Wood, S.M., 2000. Modelling and smoothing parameter estimation with multiple quadratic penalties. J. Roy. Stat. Soc. B 62 (2), 413–428.